*FAST FREQUENCY TRACKING ALGORITHM FOR OFDM APPLICATIONS

Jing Lei and Tung-Sang Ng

Department of Electrical and Electronic Engineering
The University of Hong Kong
Pokfulam Road, Hong Kong

Phone: +852++28578418, Fax: +852++25598738

ABSTRACT

In this paper, we present a fast frequency tracking algorithm for orthogonal frequency division multiplexing (OFDM) applications. Based on a novel cost function of the carrier frequency offset (CFO), an improved gradient method is proposed to construct the recursive formula. The modified S curve is also employed for the purpose of accelerating frequency tracking. Performance of the proposed algorithm is investigated analytically as well as by simulation. In comparison to the previous methods, the proposed method has faster tracking speed, larger tracking range and lower implementation complexity.

1. INTRODUCTION

Orthogonal frequency division multiplexing (OFDM) has been suggested and standardized for a variety of applications such as terrestrial and satellite digital audio broadcasting, digital television broadcasting and wireless local area networks. As a broadband transmission scheme of high spectral efficiency, OFDM is robust against many channel impairments [1], and thereby significantly reduces the complexity of receivers. However, OFDM is susceptible to the carrier frequency offset (CFO) arising from transceiver oscillator mismatches and/or Doppler shifts, which may lead to the loss of subchannel orthogonality and the severe degradation of system performance [2]. Therefore, frequency synchronization is one of the fundamental tasks performed by OFDM receivers. Generally, the process of frequency synchronization is split into an acquisition mode and a tracking mode, and different algorithms are employed in these two modes to accommodate their different requirements [3-8]. In this paper, we only address the issue of frequency tracking.

In [6], a feedback frequency synchronizer based on maximum- likelihood principle is discussed by Daffara and Chouly. The computation load of this method is heavy due to the two Fast Fourier Transform (FFT) operations required by each iteration. Another frequency tracking scheme is introduced by Daffara and Adami in [7], which exploits the redundancy associated with the cyclic prefix. In comparison with [6], the computation burden of [7] is reduced but the tracking range is decreased as well. In [8], Morelli, D'Andrea and Mengali make different mathematical approximation to the cost function developed by [6] and obtain a simplified recursive formula. Due to the narrow convexity region of their cost function, the tracking range of both [7] and [8] is limited to a fraction of the subchannel spacing. Additionally, their tracking speed is relatively slow as a result of the non-uniform restoring force of their S curve.

In this paper, a fast frequency tracking algorithm with larger tracking range and lower implementation complexity is proposed. Based on the CFO-induced phase rotation, a novel cost function about the CFO is developed, and the issue of frequency tracking is simplified into the recursive maximization of this cost function. To accomplish fast frequency synchronization, methods for accelerating the tracking process are also discussed.

The rest of this paper is organized as follows. Section 2 describes the system model and discusses the formulation of the novel cost function. Section 3 presents the new frequency tracking algorithm. Performance analysis of the proposed algorithm is conducted in Section 4. Finally, conclusions are drawn in Section 5.

2. SYSTEM MODEL AND PROBLEM FORMULATION

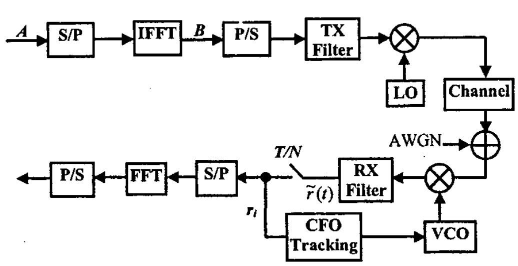

Fig.1 OFDM System Model

The system model of OFDM is shown in Fig.1. Let $A=\{a_0\ a_1\ \dots\ a_{N-1}\}$ denote the frequency-domain samples of the pilot OFDM symbol, where N is the number of subchannels. The inverse FFT (IFFT) is applied to A and the resultant sequence represented by $B=\{b_0\ b_1\ \dots\ b_{N-1}\}$ is passed through the transmitter filter to form the baseband signal. The baseband signal is then up-converted to the

* This work was supported by the Hong Kong Research Grants Council and by the University Research Committee of the University of Hong Kong..

radio frequency (RF) and transmitted through the channel. Also added into this channel is the additive white Gaussian noise (AWGN). At the receiver, the signal is down converted by the local VCO and the CFO is assumed to be f_d Hz. After passing through the receiver filter, the demodulated signal is given by

$$\tilde{r}(t) = K\exp[j(2\pi f_d t+\theta_0)]\sum_{n=0}^{N-1} b_n p(t-nT/N) + \tilde{w}(t), \quad (1)$$

where K is a constant, θ_0 is the phase difference between the local oscillator and the received symbol, $p(t)$ denotes the combined impulse response of the transceiver filters and the channel, T is the OFDM symbol period and $\tilde{w}(t)$ is the complex Gaussian noise. Signal $\tilde{r}(t)$ is sampled at the interval of T/N and the resultant N samples are represented by $\{r_i; i=0,1\dots N-1\}$. Assuming $p(t)$ satisfies the Nyquist pulse-shaping criterion for zero ISI [9] and (1) is sampled at the optimum instants, then r_i takes the form of

$$r_i = Kb_i\exp[j(\theta_0+2\pi i f_d T/N)] + w_i, \quad (2)$$

where $\{w_i\}$ are the samples of $\tilde{w}(t)$, which have zero mean and variance $2\sigma^2$. Evidently, the exponential part of (2), which represents the CFO-induced phase rotation, is proportional to f_d and can be exploited for CFO estimation. Besides, (2) also includes a factor b_i, which is independent of f_d and should be eliminated if we desire to obtain the interested part $\exp[j(\theta_0+2\pi i f_d T/N)]$ only. Since $\boldsymbol{B}$ is the IFFT of the pilot symbol, it is known by the receiver. Thus, we can obtain the desired component as follows:

$$C_i = r_i b_i^* \big/ |b_i|^2 . \quad (3)$$

By ignoring the noise term w_i in r_i, (3) can be rewritten as

$$C_i = K\exp[j(\theta_0+2\pi i f_d T/N)] . \quad (4)$$

Then, we introduce a new variable ψ defined by

$$\psi = \left| N^{-1}\sum_{i=0}^{N-1} C_i \right|^2 . \quad (5)$$

Substituting (4) into (5) yields

$$\psi = \begin{cases} |K|^2, & f_d T = mN \text{ and } m \in Z; \\ \left| K\sin(\pi f_d T)[N\sin(\pi f_d T/N)]^{-1} \right|^2, & \text{otherwise}; \end{cases} \quad (6)$$

where Z denotes the set of integers. It can be found from (6) that ψ is independent of θ_0 and the maxima of ψ occurs

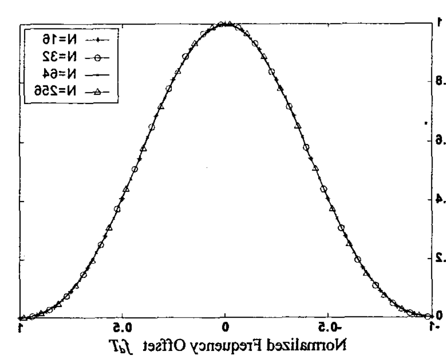

Fig.2 The relationship between ψ and f_d

at f_d=0.

Fig.2 shows the relationship between ψ and f_d for the range of $f_d \in [-T^{-1}, T^{-1}]$, with N as a parameter. For the convenience of subsequent discussions, the frequency offset is normalized by T^{-1} and the coefficient $|K|^2$ is normalized to 1. It is evident from this figure that for $f_dT \in [-1,1]$, ψ is a convex function of f_d and its shape changes little when $N \geq 16$ [11,14]. Since the objective of frequency tracking is to bring f_d to zero, maximizing ψ will eventually lead to f_d=0, the desired result, provided $|f_d|<T^{-1}$. The following section will focus on the discussion of the frequency tracking algorithm based on the factor ψ.

3. FREQUENCY TRACKING ALGORITHM

Employing ψ as the cost function of f_d, the issue of frequency tracking can be simplified into the recursive maximization of ψ with respect to f_d. Various approaches including steepest-descent-method (SDM) can be applied here to build the iteration formula. In this work, the differential-filtering steepest-descent-method (DFSDM) [10] is selected because of its simplicity and fast convergence. The major difference between DFSDM and SDM is that the former uses better approximation to the gradient rather than the "simple difference" adopted by the latter. As a result, DFSDM not only gains more relaxed bound on the step size but also achieves faster convergence rate, both of which are attractive for practical applications. For simplicity, "Momentum filter" [10,11], the simplest type of differential filters, is employed in the iteration formula, yielding

$$f_{d,k+1} = (\rho+1)f_{d,k} - \rho f_{d,k-1} + \mu\nabla_k , \quad (7)$$

where $0<\rho<1$ is a constant, μ is the step size, k denotes the iteration number and ∇_k represents the gradient given by

$$\nabla_k = (4\pi TN^{-1})^{-1}[\partial(\psi_k)/\partial(f_{d,k})], \quad (8)$$

where $\psi_k \overset{\Delta}{=} \psi\big|_{f_d=f_{d,k}}$. Inserting (5) into (8) leads to

$$\nabla_k = -N^{-2}\mathrm{Im}[\sum_{i_1=0}^{N-1} i_1 C_{i_1} \sum_{i_2=0}^{N-1} C_{i_2}^*] = -N^{-2}\mathrm{Re}[\sum_{i_1=0}^{N-1} C_{i_1} \sum_{i_2=0}^{N-1} i_2 C_{i_2}^*], \quad (9)$$

where Im(.) and Re(.) represent the imaginary part and real part of the enclosed variable, respectively, and the superscript * denotes complex conjugate.

Let $Z_k = N^{-1}\sum_{i_1=0}^{N-1} C_{i_1}\big|_{f_d=f_{d,k}}$ and $W_k = N^{-1}\sum_{i_1=0}^{N-1} i_1 C_{i_1}\big|_{f_d=f_{d,k}}$, (8) can be realized through

$$\nabla_k = -\mathrm{Im}(Z_k^* W_k) . \quad (10)$$

It is well known that S curve is the key characteristic curve to determine the performance of frequency tracking, which can be expressed as a function of f_d, say $S(f_d)$ [7]. The S curve corresponding to algorithm (7) can be expressed as

$$S(f_d) = E[\nabla_k]\big|_{f_{d,k}=f_d}$$
$$= -N^{-2}\,\mathrm{Im}\left[\frac{1-e^{-j2\pi f_d T}}{1-e^{-j2\pi f_d T/N}} \sum_{n=0}^{N-1} n e^{j2\pi f_d T/N}\right] . \quad (11)$$

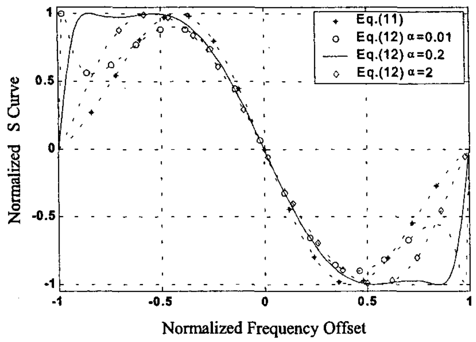

Fig.3 S Curves of Eq.(11) and (12)

Equation (11) is normalized and plotted in Fig.3 for $f_dT\in[-1, 1]$. It is noted that this S curve has a similar shape to those presented in [6-8]. An obvious drawback associated with these S curves is that their magnitude is not uniformly distributed over the tracking range and decreases monotonically when $|f_d|$ goes beyond the frequency locations of their local extrema. Consequently, even if f_d beyond such thresholds can be tracked, the tracking process is lengthy due to the small restoring force of $S(f_d)$ at the beginning. Actually, this situation often occurs when the tracking mode first takes over from the acquisition mode.

To circumvent this drawback, we propose to modify the S curve by

$$S^{\#}(f_d)=\kappa(f_d)S(f_d), \tag{12}$$

where $\kappa(f_d)$ is a f_d-dependent factor used to reshape $S(f_d)$, and $S^{\#}(f_d)$ represents the modified S curve. To maintain the polarity of $S(f_d)$, the condition of $\kappa(f_d)>0$ for $|f_d|\le T^{-1}$ should be satisfied.

A convenient way of shifting the thresholds of $S(f_d)$ towards $\pm T^{-1}$, the bounds of tracking range (see Section 4.1 for details), is to multiply it by the reciprocal of $\mathrm{Re}(Z_kW_k^*)+\alpha$, where α is a positive constant. For notational convenience, the time index k is omitted from Z_k and W_k in the following wherever appropriate.

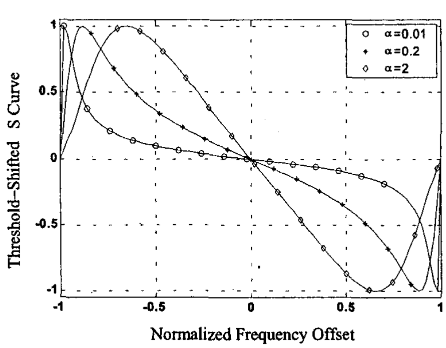

Fig.4 The effect of α on the threshold shifting of S curve

Fig.4 plots the normalized curve of $\frac{S(f_d)}{\mathrm{Re}(ZW^*)+\alpha}$ for different values of α. From this figure, we observe that as α decreases, the thresholds shift towards $\pm T^{-1}$. Nevertheless, some quantity still needs to be added to the reciprocal in order to obtain a modified S curve with uniform magnitude. For this reason, a simple but effective $\kappa(f_d)$ takes the form of

$$\kappa(f_d)=\beta+\left.\frac{\gamma}{\mathrm{Re}(Z^*W)+\alpha}\right|_{f_{d,k}=f_d}, \tag{13}$$

where β and γ are two positive constants that are dependent on α. For the purpose of normalization, β and γ are calculated by $\beta=(\lambda_1\lambda_3)^{-1}$ and $\gamma=(\lambda_2\lambda_3)^{-1}$, where $\lambda_1=\max_{f_d}[S(f_d)]$, $\lambda_2=\max_{f_d}\{\frac{S(f_d)}{\mathrm{Re}(E[Z^*W])+\alpha}\}$ and $\lambda_3=\max_{f_d}\{\frac{S(f_d)}{\lambda_1}+\frac{S(f_d)}{\lambda_2\,\mathrm{Re}(E[Z^*W])+\alpha}\}$. The characteristics of $S^{\#}(f_d)$ depend on the choice of α. If α is chosen too large, the shape of $S^{\#}(f_d)$ reduces to that of $S(f_d)$ and there is not much improvement. On the other hand, if α is too small, the shape of $S^{\#}(f_d)$ oscillates, which is undesirable as well. Since (13) is a nonlinear function of f_d, theoretical determination of suitable α is a prohibiting task Thereby, computer simulation has been conducted to find the proper range for α, which indicates the appropriate choice should be $\alpha\in(0.15, 0.25)$. To illustrate the impact of $\kappa(f_d)$, $S^{\#}(f_d)$ is also plotted in Fig.3 for α=0.01,0.2 and 2. The choice of α=0.2 results in a close to ideal S curve (square wave), whereas the curves for α=0.01 and α=2 reflect two non-ideal cases resulted from inappropriate choice of α.

Inserting (13) into (7) finally leads to the feedback frequency tracking algorithm proposed in this paper:

$$f_{d,k+1}=(\rho+1)f_{d,k}-\rho f_{d,k-1}+\mu\kappa(f_{d,k})\nabla_k \ . \tag{14}$$

In contrast to [6] and [8], no FFT operation is involved in generating the error signal ∇_k as well as the modification factor $\kappa(f_{d,k})$. Combining (8), (12) and (14), it is found that each iteration of the proposed algorithm requires a total of ($4N$+9) real multiplications and ($4N$+2) real additions. Consequently, the implementation complexity of the proposed method is much lower than that of [6] and [8].

4. PERFORMANCE ANALYSIS

4.1 Tracking Range

Let $f_{d\max}$ and $f_{d\min}$ denote the upper and lower frequency bound within which the tracking algorithm is effective, and the tracking range can then be given by $f_{d\max}-f_{d\min}$. To find the tracking range of the proposed algorithm, we substitute (13) into (12) and obtain

$$S^{\#}(f_d)=N^{-2}\kappa(f_d)\,\mathrm{Im}\left[\frac{1-e^{-j2\pi f_dT}}{1-e^{-j2\pi f_dT/N}}\sum_{n=0}^{N-1}ne^{j2\pi f_dT/N}\right]. \tag{15}$$

For (15), the first pair of zero-crossing points with opposite signs are located at $f_{d\max}=T^{-1}$ and $f_{d\min}=-T^{-1}$. Therefore, the tracking range of the proposed algorithm is $T^{-1}-(-T^{-1})=2T^{-1}$, which equals twice the symbol rate of the OFDM system.

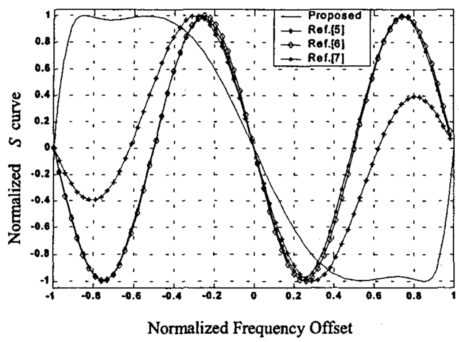

Fig.5 Normalized S Curves of different feedback CFO tracking algorithms

To compare the tracking range of the proposed algorithm and other feedback schemes [6-8], their normalized S curves are all shown in Fig.5. It can be seen from this figure that the proposed algorithm has significantly larger tracking range than previous methods that can track CFO in a fraction of the subchannel spacing only.

4.2 Transient Tracking Behavior

To illustrate the efficacy of the modified S curve $S^{\#}(f_d)$, simulations are carried out to compare the performance of algorithm (7) and algorithm (14). Unless otherwise stated, α=0.2 is employed by the reshaping function given by (13) in the following simulations. Fig.6 plots trajectories of transient tracking behavior for both algorithms under E_s/N_0=0dB, where $E_s/N_0 \overset{\Delta}{=} |K|^2(N\sigma^2)^{-1}\sum_{i=0}^{N}|b_i|^2$. The system parameters used in this experiment are:

T=(5×10^6 symbols/second)$^{-1}$,
$f_{d,0}T$=–0.99,
μ=0.01,
N=512.

It can be observed from Fig.6 that (14) settles to the steady state much faster than (7), which demonstrates the modified S curve $S^{\#}(f_d)$ has faster tracking speed than its counterpart $S(f_d)$ due to its more uniform restoring force.

4.3 Steady-State Tracking Behavior

In order to analyze the steady-state tracking behavior of the proposed method, ∇_k is split into a deterministic part $S(f_{d,k})$ and a random part $\hat{w}_k$. Hence, (14) can be rewritten as

$$f_{d,k+1}=(1+\rho)f_{d,k}-\rho f_{d,k-1}+\mu S^{\#}(f_{d,k})+\mu\kappa(f_{d,k})\hat{w}_k\,, \quad (16)$$

where $\hat{w}_k$ can be expanded into

$$\hat{w}_k=N^{-1}\left\{\sum_{m=0}^{N-1}w_{I,m}(W_{Q,k}-mZ_{Q,k})-\sum_{n=0}^{N-1}w_{Q,n}(W_{I,k}-nZ_{I,k})\right\} - N^{-2}\sum_{n=0}^{N-1}\sum_{m=0}^{N-1}w_{I,m}w_{Q,n}(m-n)\quad, \quad (17)$$

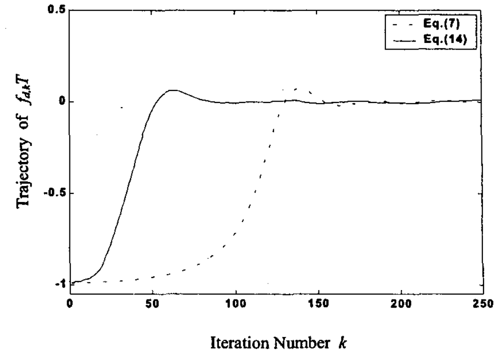

Fig.6 Transient tracking behaviors of algorithm (7) and (14) under E_s/N_0=0 dB

and the variables in the form of $X_{I,l}$ and $X_{Q,l}$ denote Re(X_l) and Im(X_l), respectively. Following the standard method of [11-13], the first and second moments of $\hat{w}_k$ are found to be

$$E[\hat{w}_k]=0 \quad (18)$$

and

$$E[\hat{w}_k\hat{w}_{k+p}]=\delta(p)\{\sigma_0^2N^{-4}\sum_{n_1=0}^{N-1}\sum_{n_2=0}^{N-1}\sum_{n_3=0}^{N-1}(n_2n_3+n_1^2-2n_1n_2)\cos[2\pi Tf_{d,k}(n_2-n_3)/N]+\sigma_0^4(6N^2)^{-1}(N^2-1)\}, \quad (19)$$

respectively, where $\delta(p)$ is the Kronecker function. When p=0 and $f_{d,k}$ is sufficiently small, (19) reduces to

$$\lim_{f_{d,k}\to 0}E[\hat{w}_k^2]\approx(N+2\sigma^2)(N^2-1)(12N^2)^{-1}\sigma^2. \quad (20)$$

Since we are interested in the steady-state behavior only, the assumption $f_{d,k}\approx 0$ is well justified in obtaining (20). Furthermore, (16) can be approximated linearly by

$$f_{d,k+1}=(1+\rho+\mu K_A)f_{d,k}-\rho f_{d,k-1}+\mu\kappa_0\hat{w}_k\,, \quad (21)$$

where $K_A \overset{\Delta}{=} \lim_{f_d\to 0}\partial[S^{\#}(f_d)]/\partial(f_d)$ and $\kappa_0 \overset{\Delta}{=} \kappa(0)$. It follows from (21) that $\{\hat{w}_k\}$ and $\{f_{d,k}\}$ can be viewed as the input and output of a linear system with the transfer function of

$$Q(z^{-1})=\frac{\mu\kappa_0 z^{-1}}{1-(1+\rho+\mu K_A)z^{-1}+\rho z^{-2}}\,. \quad (22)$$

In accordance with [11], we have

$$E[f_d]=0 \quad (23)$$

and

$$E[f_{d,k}f_{d,k+p}]=E[\hat{w}_k\hat{w}_{k+p}]\Theta R_{QQ}(p)\,, \quad (24)$$

where the operator Θ denotes discrete convolution,

$$R_{QQ}(p)=(\bar{A}+\bar{B})r_1^{p}\varepsilon(p)+(\bar{B}+\bar{C})r_2^{p}\varepsilon(p) +(\bar{A}+\bar{B})r_1^{-p}\varepsilon(-p-1)+(\bar{B}+\bar{C})r_2^{-p}\varepsilon(-p-1)\,, \quad (25)$$

$$\varepsilon(p)=\begin{cases}1 & p\geq 0\\ 0 & p<0\end{cases}\,, \quad (26)$$

r_1 and r_2 being the roots of equation $r^2-(1+\rho+K_A)r+\rho=0$, $\bar{A}=\frac{\kappa_0^2\mu^2r_1^2}{(r_1-r_2)^2(1-r_1^2)}$, $\bar{B}=\frac{\kappa_0^2\mu^2r_1r_2}{(r_1-r_2)^2(r_1r_2-1)}$ and $\bar{C}=\frac{\kappa_0^2\mu^2r_2^2}{(r_1-r_2)^2(1-r_2^2)}$.

Particularly, the variance of f_d is given by

$$\sigma_{f_d}^2 = \sigma_{\hat{w}}^2 R_{QQ}(0) = \sigma_{\hat{w}}^2 (\overline{A} + 2\overline{B} + \overline{C}). \quad (27)$$

Equation (23) indicates the proposed method is unbiased. Besides, $\sigma_{f_dT}^2$, the normalized variance of steady-state frequency jitter [8], can be obtained by

$$\sigma_{f_dT}^2 = T^2 \sigma_{f_d}^2. \quad (28)$$

The steady-state tracking behavior of those algorithms in [6-8] can also be evaluated by invoking the linearization approach above. Fig.7 shows $\sigma_{f_dT}^2$, the normalized variance of frequency jitter, as a function of E_s/N_0 for the proposed algorithm and those presented by [6-8] over the AWGN channel. The subchannel utilization efficiency [6-8] is assumed to be 1 and the number of guard interval samples [7] is set to 50. The other system parameters used in this simulation are the same as those in obtaining Fig.6. Monte Carlo (MC) simulation is also carried out to calculate the time average of $\sigma_{f_dT}^2$ and the simulation result of 10^4 runs is represented by circles in Fig.7. Examination of this figure indicates that the MC simulation result agrees well with the analytical analysis (28). Moreover, the proposed method has smaller variance than [6] and [7], and its accuracy is comparable to that of [8].

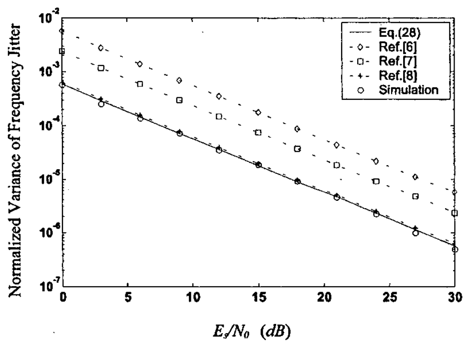

Fig.7 Normalized variance of frequency jitter for the proposed algorithm and those presented by [6-8]

5. CONCLUSION

In this paper, a fast feedback frequency tracking algorithm has been proposed for OFDM applications. A novel cost function of CFO has been developed and a simple type of differential filtering steepest descent method has been selected to construct the recursive formula. To further accelerate the speed of frequency tracking, the modification of S curve has been discussed and a simple but effective reshaping function has been derived. Performance of the proposed method has been analyzed and compared with previous feedback schemes presented by [6-8].

REFERENCES

[1] J. A. C. Bingham, "Multicarrier modulation for data transmission: An idea whose time has come," *IEEE Commun. Mag.*, Vol. 28. pp. 5-14, May 1990.

[2] T. Pollet, M. Blade and M. Moeneclaey, "BER sensitivity of OFDM systems to carrier frequency offset and Weiner phase noise," *IEEE Trans. Commun.*, Vol. 43, pp. 191-193, Feb./Mar./Apr. 1995.

[3] T. M. Schmidl and D. C. Cox, "Robust frequency and timing synchronization for OFDM," *IEEE Trans. Commun.*, Vol.45, pp. 1613-1621, Dec. 1997.

[4] M. Luise and R. Reggiannini, "Carrier frequency acquisition and tracking for OFDM systems," *IEEE Trans. Commun.* , Vol.44, pp. 1590-1598, Nov. 1996.

[5] M. Morelli and U. Mengali, "An improved frequency offset estimator for OFDM applications," *IEEE Commun. Letters*, Vol.3, pp. 75-77, Mar. 1999.

[6] F. Daffara and A. Clouly, "Maximum likelihood frequency detectors for orthogonal multicarrier systems," *Proc. ICC'93*, pp. 766-771, Jun. 1993.

[7] F. Daffara and O. Adami, "A novel carrier recovery technique for orthogonal multicarrier systems," *Eur. Trans. Telecommun.*, Vol.7, pp. 324-334, Jul.-Aug., 1996.

[8] M. Morelli, A. N. D'Andrea and U. Mengali, "Feedback frequency synchronization for OFDM applications," *IEEE Commun.Letters*, Vol. 5, pp. 28-30, Jan. 2001.

[9] J. G. Proakis, Digital Communications, Third Edition, McGraw-Hill Inc., 1995.

[10] V. Solo and X. Kong, Adaptive Signal Processing Algorithms, Prentice Hall, Inc., Englewood Cliffs, NJ, 1995.

[11] J. Lei and T. S. Ng, "New AFC algorithm for a fully-digial DS/CDMA Receiver", *Proc. of IEEE ISCAS'01*, Vol.4, pp. 294-297.

[12] A. V. Oppenheim and R. W. Schafer, Discrete-Time Signal Processing, Prentice Hall, Inc., Englewood Cliffs, NJ, 1989.

[13] S. M. Kay, Fundamentals of Statistical Signal Processing: Estimation Theory, Prentice Hall, Inc., Englewood Cliffs, New Jersey, 1993.

[14] A. Q. Hu, P. C. K. Kwok and T. S. Ng, "MPSK DS/CDMA carrier recovery and tracking based on correlation technique", *IEE Electronics Letters*, Vol.35, No.3, pp.201-203, Feb. 1999.